Faraday Discussions

New Interstellar Laboratories in the Molecular Ring: Electronic Supplementary Information

Olivia H. Wilkins*‡ and Geoffrey A. Blake

We conducted a pilot survey of 11 giant molecular clouds (GMCs) using the Atacama Compact Array (ACA), a subset of dedicated Atacama Large Millimeter/submillimeter Array (ALMA) antennas. GMCs in the sample were selected for their high mass surface density and location in the so-called molecular ring. Furthermore, sources in the sample had not been previously observed in the context of molecular line emission prior to this work. Within the sample, ≥ 15 (candidate) molecular cores were identified based on $C^{18}O$ and CH_3OH emission that was cospatial with 1.2 mm continuum emission. All objects with both $C^{18}O$ and CH_3OH emission correspond to previously identified young stellar objects (YSOs) and YSO candidates. Nine target GMCs contained fittable methanol (CH_3OH) emission, from which rotation temperature and column density maps were derived. Differences in chemical diversity, derived CH_3OH rotation temperature, and SiO emission suggest that surveyed objects represent a range of evolutionary stages. This work lays the foundation for follow-up high-angular-resolution studies of the gas-phase chemistry.

The Supplementary Information in this document includes observation details (Section S1), an explanation for distance uncertainty calculations (Section S2), and propagated CH_3OH rotation temperature and column density uncertainty maps (Section S3).

S1 Observation Details

An overview of the 1.2 mm ALMA observations is provided in Section 3 of the main text. This manuscript focuses on data from ACA Band 6 observations. Here we detail the ACA observations toward each source, identified by BGPS ID, in both the "lower" ($\sim$226 GHz) and "upper" ($\sim$251 GHz) local oscillator (LO) settings to complement the target and image properties listed in Tables 1 and 2 as well as to introduce the complete data set for ALMA project #2018.1.01259. The data set also incorporates observations with the Total Power (TP) Array, which uses up to four 12-meter antennas that act as a single dish telescope; TP observations are outlined here for reference in future work.

California Institute of Technology, 1200 East California Boulevard, Pasadena CA 91125, USA.

* Corresponding author. Permanent E-mail: olivia.h.wilkins@outlook.com

‡ Present address: NASA Postdoctoral Program Fellow, NASA Goddard Space Flight Center, 8800 Greenbelt Road, Greenbelt MD 20771, USA. E-mail: olivia.h.wilkins@nasa.gov

S1.1 BGPS 3053

ACA observations toward BGPS 3053 consisted of 105 pointings. From the lower Band 6 observations, two executed observing blocks were used for imaging, with 10 antennas on 2019 April 28 and 9 antennas on 2019 April 29, both with a time on source of ~4000 seconds. A third execution block with 9 antennas on 2019 April 29 was disregarded in data imaging because it was terminated early after ~2210 seconds and thus does not incorporate all pointings over BGPS 3053. Upper Band 6 ACA data were taken from two execution blocks with 10 antennas each on 2019 May 05. These observations use J1832-1035 as a phase and WVR calibrator and J1924-2914 as an atmospheric, bandpass, flux, pointing, and WVR calibrator.

TP observations in lower Band 6 were taken over four execution blocks using 3 antennas on 2019 March 12, 3 antennas on 2019 March 17, and two blocks of 4 antennas on 2019 May 03 (one of which was at low elevation). In upper Band 6, there were three TP execution blocks of 4 antennas on 2019 May 06 and May 25 and 3 antennas on 2019 June 01.

S1.2 BGPS 3474

ACA observations toward BGPS 3474 consisted of 115 pointings. The lower Band 6 observations were carried out in two execution blocks of ten antennas each on 2019 May 22. Upper Band 6 observations were made in two execution blocks of 11 antennas on 2019 May 25 and 10 antennas on 2019 May 29. J1832-1035 was used as a phase and WVR calibrator, J1924-2914 was used as an atmospheric, bandpass, flux, pointing, and WVR calibrator.

Lower Band 6 TP observations were taken over four execution blocks, three with 3 antennas on 2019 June 02 and one with 3 antennas on 2019 June 03. The upper band 6 TP observations were taken using 2 antennas on 2019 August 21 and 3 antennas on 2019 September 25; these data have baseline residuals due to precipitable water vapor (0.5 and 1.8 mm, respectively).

S1.3 BGPS 4449

ACA observations toward BGPS 4449 consisted of 105 pointings. In the lower Band 6 observations, two execution blocks were carried out on 2019 May 20 with 11 antennas each. Upper Band 6 observations were made with 11 antennas on 2019 May 25 and 10 antennas on 2019 May 29. J1851+0035 was used as a phase, pointing, and WVR calibrator, and J1907+0127 was used as an

atmospheric, phase, and WVR calibrator.

TP observations in lower Band 6 were made over four execution blocks of 2 antennas each between 2019 August 20 and 2019 August 27. Three execution blocks of 2 antennas each on 2019 August 19-20 for upper Band 6. To avoid galactic contamination, the off-pointing positions for calibrating the TP observations were made about $3.5''$ away, which is not ideal for calibration and results in noisy baselines in some of the spectral windows.

S1.4   BGPS 5623

ACA observations toward BGPS 5623 were made with 105 pointings. Lower Band 6 ACA observations were carried out with two execution blocks of 10 antennas on 2019 May 05. This was the same for upper Band 6 but on 2019 May 22 and 29. J1924-2914 was used as an atmospheric, bandpass, flux, pointing, and WVR calibrator, and J1851+0035 was used as a phase, pointing, and WVR calibrator.

Lower Band 6 TP observations were carried out with three execution blocks of 4 antennas each on 2019 May 04, 05, and 06. Upper Band 6 observations were carried out in three execution blocks of 2 antennas each on 2019 August 15 and 17.

S1.5   BGPS 6029

ACA observations toward BGPS 6029 were made with 85 pointings. Lower Band 6 observations were carried out in two execution blocks of 11 antennas each on 2019 May 12 and 18. Upper Band 6 ACA observations were carried out in two execution blocks of 10 antennas each on 2019 May 21-22. J1851+0035 was used as an atmospheric, phase, and WVR calibrator, and J1924-2914 was used as an atmospheric, bandpass, flux, pointing, and WVR calibrator.

TP observations in lower Band 6 were carried out in two execution blocks of 3 antennas each on 2019 June 04. Upper Band 6 TP observations were carried out in two execution blocks with 3 antennas on 2019 June 04 and 2 antennas on 2019 August 07.

S1.6   BGPS 6082, BGPS 6112, BGPS 6299, and BGPS 6318

BGPS 6082, BGPS 6112, BGPS 6299, and BGPS 6318 were all observed during the same execution blocks. ACA lower Band 6 observations were taken during two execution blocks of 9 antennas each on 2019 April 29 and 2019 May 01. Upper band 6 observations were taking in two execution blocks of 9 antennas each on 2019 May 02-03. J1935+2031 was used as an atmospheric, phase, and WVR calibrator, and J1924-2914 was an atmospheric, bandpass, flux, pointing, and WVR calibrator.

There were five TP execution blocks in lower Band 6 of 4 antennas on 2018 October 28, 4 antennas on 2019 March 22, 3 antennas on 2019 April 09, 4 antennas on 2019 April 17, and 4 antennas on 2019 April 22. In upper Band 6, there were four execution blocks of 3 antennas on 2019 April 30, 3 antennas on 2019 May 01, and two blocks of 4 antennas on 2019 May 04.

S1.7   BGPS 6120

ACA observations of BGPS 6120 were carried out in 105 pointings. In the lower band, there were two execution blocks of 9 antennas on 2019 May 03 and 11 antennas on 2019 May 04. Upper Band 6 observations were carried out in two execution blocks of 11 antennas on 2019 May 11 and 18. J1924-2914 was used as an atmospheric, bandpass, flux, pointing, and WVR calibrator; J1935+2031 was used as an atmospheric, phase, and WVR calibrator.

TP observations in lower Band 6 consisted of three execution blocks of 3 antennas on 2019 May 29, 4 antennas on 2019 June 02, and 3 antennas on 2019 June 04. Two executions of upper Band 6 TP observations were attempted but did not pass quality assurance. Therefore, there are not TP data for the upper Band 6 toward BGPS 6120.

S1.8   BGPS 6310

ACA observations toward BGPS 6310 were carried out with 105 pointings. Lower Band 6 observations were carried out in two execution blocks of 9 antennas on 2019 May 02-03. Upper Band 6 ACA observations were taken with 11 antennas during two execution blocks on 2019 May 04. Calibrators were J1924-2914 for atmosphere, bandpass, flux, pointing, and WVR; J1924+1540 for pointing and WVR; and J1935+2031 for atmosphere, phase, and WVR.

TP observations in the lower band were carried out in three execution blocks with 3 antennas each on 2019 April 27-28 and 2019 May 02. Upper Band 6 TP observations were taken in three execution blocks of 4 antennas on 2019 May 25, 2 antennas on 2019 May 31, and 3 antennas on 2019 June 01.

S2   Calculating Distance Uncertainty

The kinematic distances d_{kin} reported by Battisti and Heyer[1] were calculated using the size-velocity dispersion relationship for molecular clouds

$$D_{svd} = \frac{1}{\theta} \left(\frac{\Sigma_{GMC}}{100 \, M_\odot \ \mathrm{pc}^{-2}} \right)^{-1} \left(\frac{\sigma_v}{v_o} \right)^2 \ \mathrm{pc} \qquad (1)$$

where θ is the angular radius of the cloud in radians, Σ_{GMC} is the surface density of the cloud in $M_\odot \ \mathrm{pc}^{-2}$, σ_v is the velocity dispersion, $v_o = 0.7 \pm 0.07 \ \mathrm{km \ s}^{-1} \ \mathrm{pc}^{-1/2}$ [2] is defined by

$$v_o = \frac{\sigma_v}{\Sigma_{GMC} R}^{1/2} \qquad (2)$$

for cloud size R and is nearly constant for clouds within the disk of the Milky Way.

The propagation for uncertainty in the distance $\sigma(d_{kin})$ then follows Equation 3.

$$\sigma(d_{kin}) = |d_{kin}| \sqrt{ \left(\frac{\sigma(\Sigma_{GMC})}{|\Sigma_{GMC}|} \right)^2 + 2 \left(\frac{\sigma(\sigma_v)}{|\sigma_v|} \right)^2 + 2 \left(\frac{\sigma(v_o)}{|v_o|} \right)^2 } \quad (3)$$

The uncertainty in surface density (Equation 1 in the main text) is derived from uncertainty in GMC mass M_{GMC} and radius R_{GMC}

reported by Battisti and Heyer such that

$$\sigma(\Sigma_{GMC}) = |\Sigma_{GMC}| \sqrt{\left(\frac{\sigma(M_{GMC})}{M_{GMC}}\right)^2 + 2\left(\frac{\sigma(R_{GMC})}{R_{GMC}}\right)^2}. \quad (4)$$

The velocity dispersion σ_v and associated uncertainty for reach GMC are also taken from Battisti and Heyer, and the third term in Equation 3 is 0.02 for all GMCs. Rearranging Equation 4 and substituting that and 0.02 for the first and third terms in Equation 3, we propagate the distance uncertainty by

$$\sigma(d_{kin})$$

$$= |d_{kin}| \sqrt{\left(\frac{\sigma(M_{GMC})}{|M_{GMC}|}\right)^2 + 2\left(\frac{\sigma(R_{GMC})}{|R_{GMC}|}\right)^2 + 2\left(\frac{\sigma(\sigma_v)}{|\sigma_v|}\right)^2 + 0.02}. \quad (5)$$

S3 Rotation Temperature and Column Density Uncertainty Maps

Percent uncertainty maps were calculated from the derived `LMFIT` standard errors. These maps are presented in Figures S1-S9. For most objects, the rotation temperature and column density uncertainties are $\leq 10\%$ near the millimeter continuum emission peak for each fitted region. Higher uncertainty is seen toward the edges of the fitted regions, which is expected since the emission falls off and noiser and hence more difficult to fit robustly.

Notes and references

1 A. J. Battisti and M. H. Heyer, *Astrophys. J.*, 2014, **780**, 173.
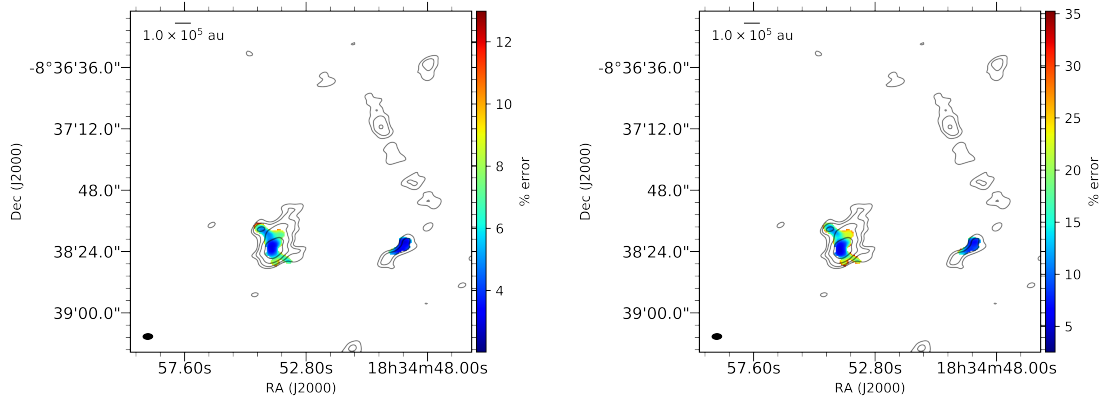2 M. Heyer, C. Krawczyk, J. Duval and J. M. Jackson, *Astrophys. J.*, 2009, **699**, 1092–1103.

Fig. S1 Percent uncertainty maps for the derived CH$_3$OH rotation temperature (left) and column density (right) in BGPS 3053.
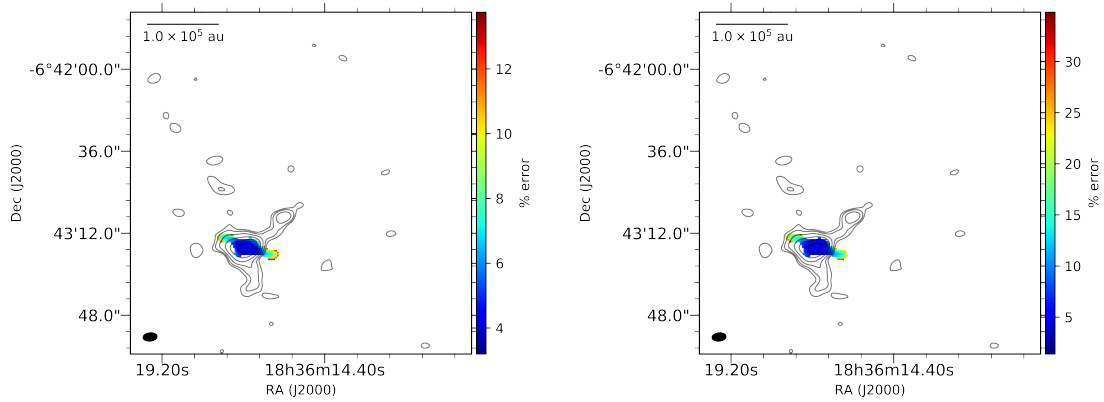

Fig. S2 Percent uncertainty maps for the derived CH$_3$OH rotation temperature (left) and column density (right) in BGPS 3474.
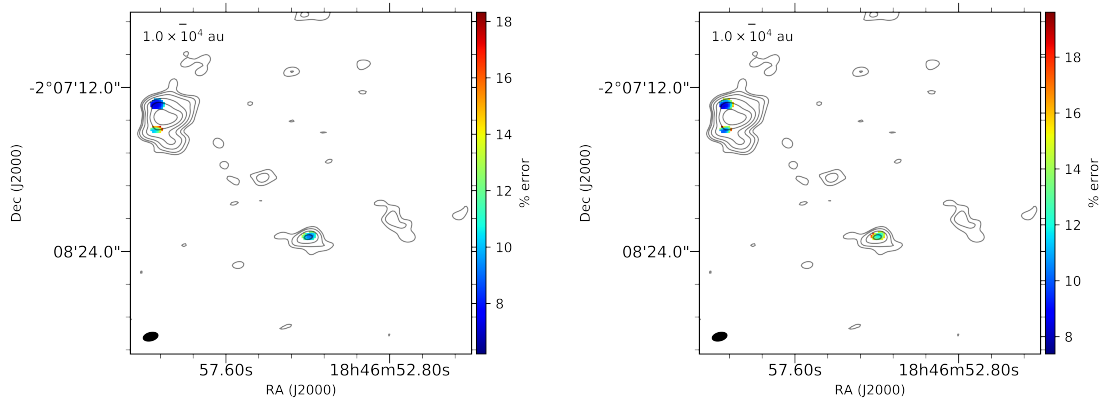

Fig. S3 Percent uncertainty maps for the derived CH$_3$OH rotation temperature (left) and column density (right) in BGPS 4449.
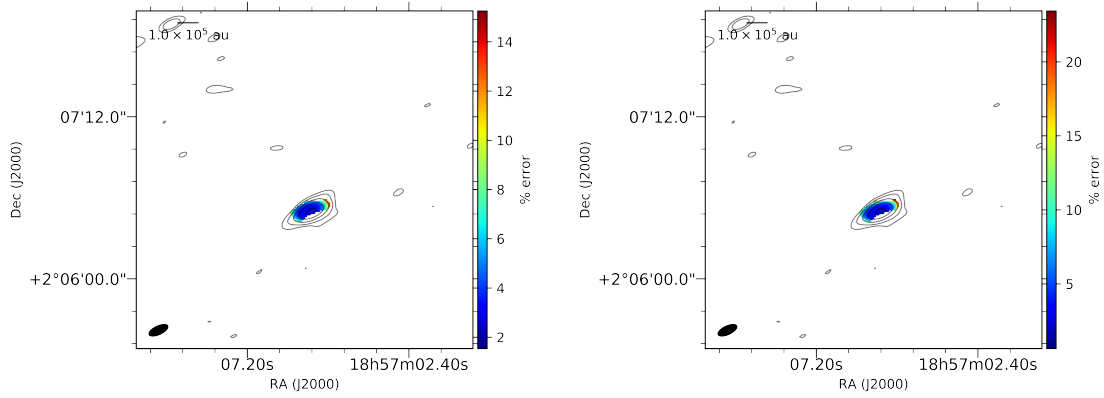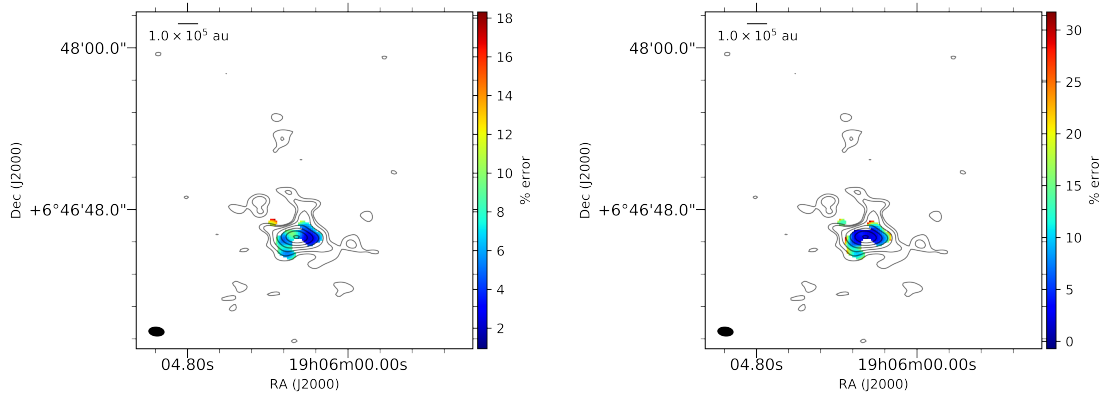
Fig. S4 Percent uncertainty maps for the derived CH$_3$OH rotation temperature (left) and column density (right) in BGPS 5623.

Fig. S5 Percent uncertainty maps for the derived CH$_3$OH rotation temperature (left) and column density (right) in BGPS 6029.
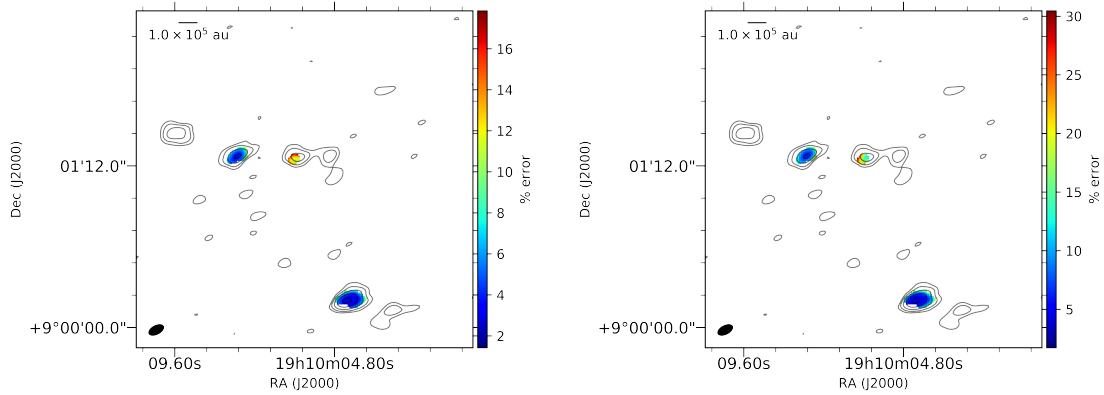

Fig. S6 Percent uncertainty maps for the derived CH$_3$OH rotation temperature (left) and column density (right) in BGPS 6112.
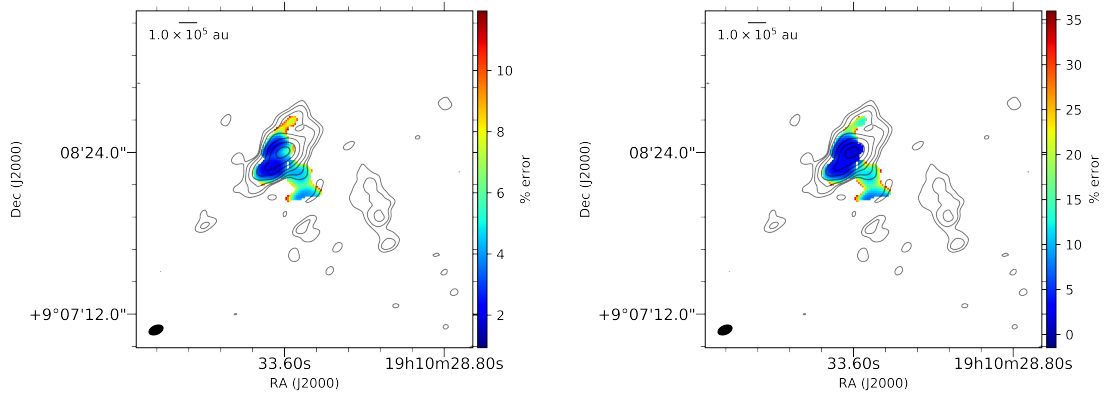
Fig. S7 Percent uncertainty maps for the derived CH$_3$OH rotation temperature (left) and column density (right) in BGPS 6120.
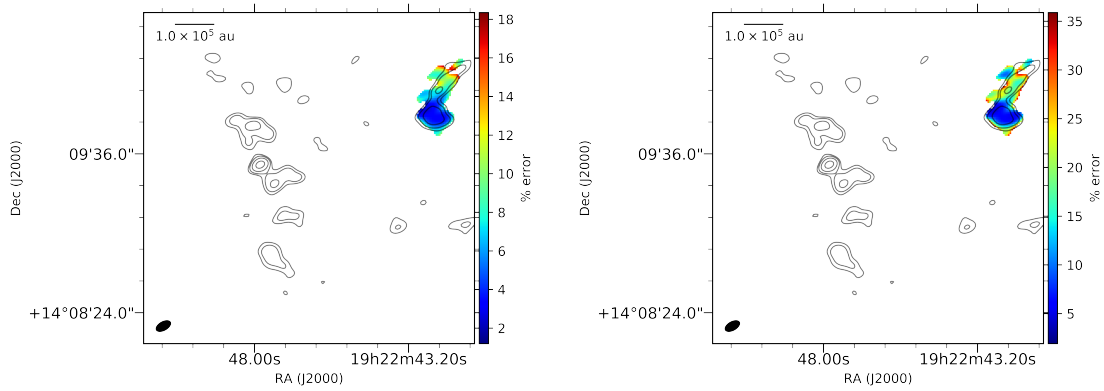

Fig. S8 Percent uncertainty maps for the derived CH$_3$OH rotation temperature (left) and column density (right) in BGPS 6299.
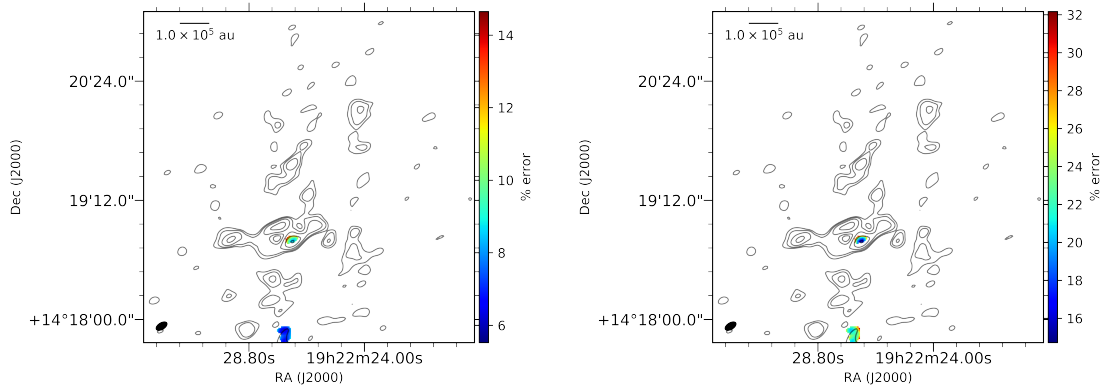

Fig. S9 Percent uncertainty maps for the derived CH$_3$OH rotation temperature (left) and column density (right) in BGPS 6310.